CMS Physics Analysis Summary

Contact: cms-pag-conveners-higgs@cern.ch 2012/11/16

Updated results on the new boson discovered in the search for the standard model Higgs boson in the $H \to ZZ \to 4\ell$ channel in pp collisions at $\sqrt{s} = 7$ and 8 TeV

The CMS Collaboration

Abstract

Measurements of the properties of the new boson recently observed at a mass near 125 GeV in the CMS experiment are reported. The results are obtained from a comprehensive search for the standard model Higgs boson in the $H \to ZZ$ decay channel, where both Z's decay to electron, muon, or tau lepton pairs. The search covers Higgs boson mass hypotheses in the range $110 < m_H < 1000$ GeV. The analysis uses pp collision data recorded by the CMS detector at the LHC, corresponding to integrated luminosities of 5.1 fb^{-1} at $\sqrt{s} = 7$ TeV and 12.2 fb^{-1} at $\sqrt{s} = 8$ TeV. The new boson is observed with a local significance above the expected background of 4.5 standard deviations. The signal strength μ, relative to the expectation for the standard model Higgs boson, is measured to be $\mu = 0.80^{+0.35}_{-0.28}$ at 126 GeV. A measurement of its mass gives 126.2 ± 0.6 (stat) ± 0.2 (syst) GeV. The hypothesis 0^+ of the standard model for the spin $J = 0$ and parity $P = +1$ quantum numbers is found to be consistent with the observation. Under the assumption that the observed boson has spin zero the data disfavor the pseudoscalar hypothesis 0^- with a CL_s value of 2.4%. No other significant excess is found, and upper limits at 95% confidence level exclude the ranges 113–116 GeV and 129–720 GeV while the expected exclusion range for the standard model Higgs boson is 118–670 GeV.

1 Introduction

The standard model (SM) of electroweak interactions [1–3] relies on the existence of the Higgs boson (H, with mass m_{H}), a scalar particle associated with the field responsible for the spontaneous electroweak symmetry breaking [4–9].

In July 2012, the CMS and ATLAS experiments announced [10, 11] the discovery of a new boson at a mass around 125 GeV, with properties compatible with the SM Higgs boson. In this paper, the properties of the new boson are studied in the channel $\mathrm{H} \to \mathrm{ZZ} \to 4\ell$ using 5.1 fb^{-1} of pp data from the LHC collected in 2011 at $\sqrt{s} = 7$ TeV, and 12.2 fb^{-1} collected in 2012 at $\sqrt{s} = 8$ TeV. The properties examined are the signal strength, relative to the expectation for the SM Higgs boson, the mass, the parity quantum number, and the corresponding fraction of a *CP*-violating contribution to the decay amplitude expressed through the fraction of the decay rate. In addition, a comprehensive search for other SM-like Higgs boson particles is performed through the $\mathrm{H} \to \mathrm{ZZ} \to 4\ell$ and $\mathrm{H} \to 2\ell 2\tau$ channels. The analysis is optimized for a SM-like Higgs boson particle in the mass range $110 < m_{\mathrm{H}} < 1000$ GeV. Compared to the previous CMS analyses [10, 12], it relies on minor improvements in lepton reconstruction and isolation algorithm, better lepton energy and momentum resolutions, extended trigger coverage for electrons and an improved kinematical discriminant exploiting the production and decay kinematics expected for the signal events. The methods to estimate the backgrounds are unchanged.

Searches for a SM Higgs boson have been previously performed at the LHC using about 5 fb^{-1} of 2011 data, in the $\mathrm{H} \to \mathrm{ZZ} \to 4\ell$ channel ($\ell = e, \mu$) by ATLAS [13] and CMS [12], and in the $\mathrm{H} \to \mathrm{ZZ} \to 2\ell 2\tau$ channel by CMS [14]. The results from CMS excluded the SM Higgs boson in the mass range 127–600 GeV at 95% confidence level (CL) [15]. ATLAS excluded 111.4–116.6 GeV, 119.4–122.1 GeV, and 129.2– 541 GeV at 95% CL [16, 17]. Direct searches for the SM Higgs boson at the LEP $\mathrm{e}^+\mathrm{e}^-$ collider have led to a lower-mass bound of $m_{\mathrm{H}} > 114.4$ GeV [18].

The analysis presented in this paper relies critically on the reconstruction, identification, and isolation of leptons. The high lepton reconstruction efficiencies are achieved for a ZZ system composed of two pairs of same-flavour and opposite-charge isolated leptons, $\mathrm{e}^+\mathrm{e}^-$, $\mu^+\mu^-$, or $\tau^+\tau^-$, in the measurement range $m_{4\ell}, m_{2\ell 2\tau} > 100$ GeV. One or both of the Z bosons can be off-shell. The single-resonant four-lepton production ($\mathrm{Z} \to 4\ell$) is used as a standard candle in the mass range $70 < m_{4\ell} < 100$ GeV [19]. The background sources include an irreducible four-lepton contribution from direct ZZ (or $\mathrm{Z}\gamma^*$) production via $\mathrm{q\bar{q}}$ annihilation and gg fusion. Reducible contributions arise from $\mathrm{Zb\bar{b}}$ and $\mathrm{t\bar{t}}$ where the final states contain two isolated leptons and two b jets producing secondary leptons. Additional background of instrumental nature arises from Z + jets and WZ + jets events where jets are misidentified as leptons.

2 CMS detector and experimental methods

Particles produced in the pp collisions are detected in the pseudorapidity range $|\eta| < 5$, where $\eta = -\ln[\tan(\theta/2)]$ and θ is the polar angle with respect to the direction of the counterclockwise proton beam. The CMS detector comprises a superconducting solenoid, providing a uniform magnetic field of 3.8 T in the bore, equipped with silicon pixel and strip tracking systems ($|\eta| < 2.5$) surrounded by a lead tungstate crystal electromagnetic calorimeter (ECAL) and a brass-scintillator hadronic calorimeter (HCAL) covering $|\eta| < 3.0$. A steel/quartz-fiber Cherenkov calorimeter extends the coverage to $|\eta| < 5$. The steel return yoke outside the solenoid is instrumented with gas ionization detectors used to identify muons up to $|\eta| < 2.4$. A detailed description of the detector is given in Ref. [20].

A complete reconstruction of the individual particles emerging from each collision event is obtained via a particle-flow (PF) technique. This uses the information from all CMS sub-detectors to identify and reconstruct individual particles in the collision event [21, 22]. They are classified into mutually exclusive categories: charged hadrons, neutral hadrons, photons, muons, and electrons.

For electrons, reconstructed candidates are first obtained in an inclusive way to gain efficiency. The electrons are reconstructed within the geometrical acceptance, $|\eta^{\mathrm{e}}| < 2.5$, and for transverse momentum $p_{\mathrm{T}}^{\mathrm{e}} > 7\,\mathrm{GeV}$. The reconstruction combines the information from clusters of energy deposits in the ECAL and the trajectory in the inner tracker [23, 24]. The track-cluster matching is initiated either "outside-in" from energy cluster measurements, or "inside-out" from track reconstruction. Trajectories in the tracker volume are reconstructed using a dedicated modeling of the electron energy loss and fitted with a Gaussian sum filter. The contribution of the ECAL to the electron momentum and its uncertainty is determined via a multivariate regression approach. The regression is trained on non-radiating electrons in a sample of simulated events, separately for barrel and endcaps. It uses the ratio of the true electron energy to the raw reconstructed energy as the target variable. The input variables involve in particular shower-shape variables. An improvement in the resolution of the $m_{4\ell}$ reconstructed mass of the order of 10% is achieved for low mass Higgs with respect to Ref. [10], in agreement with what is observed with $Z \to ee$ events. Electron identification relies on a multivariate technique that combines observables sensitive to the amount of bremsstrahlung along the electron trajectory, the geometrical and momentum matching between the electron trajectory and associated clusters, as well as shower-shape observables. The multivariate identification is trained using a Higgs boson Monte Carlo (MC) sample for the signal and a W + 1 jet data sample for background, and the working point is optimized using a Z + 1 jet data sample.

Muons are reconstructed within $|\eta^{\mu}| < 2.4$ and for $p_{\mathrm{T}}^{\mu} > 5\,\mathrm{GeV}$ [25]. The reconstruction combines the information from both the silicon tracker and the muon spectrometer. The matching between the inner and outer tracks is initiated either "outside-in", starting from a track in the muon system, or "inside-out", starting from a track in the silicon tracker. The PF muons are selected among the reconstructed muon track candidates by applying minimal requirements on the track components in the muon system and taking into account matching with small energy deposits in the calorimeters [26].

Corrections accounting for residual differences between data and simulation are applied to the muon momentum as well as on the ECAL energy before combining with the tracking momentum for electrons.

Tau leptons are identified in their leptonic decay mode denoted τ_ℓ, with an electron or muon as measurable decay product, and in the semileptonic one denoted τ_{h}, with hadrons in the decay products. The PF particles are used to reconstruct τ_{h} with the "hadron-plus-strip" (HPS) algorithm [27]. The HPS algorithm optimizes the reconstruction and identification of specific τ_{h} decay modes. The π^0 components of the τ_{h} are first reconstructed and then combined with charged hadrons to reconstruct the τ_{h} decay modes. The neutrinos produced in all τ decays escape detection and are ignored in the reconstruction. The taus in this analysis are required to have $|\eta^{\tau_{\mathrm{h}}}| < 2.3$ and $p_{\mathrm{T}}^{\tau_{\mathrm{h}}} > 20\,\mathrm{GeV}$.

The isolation of individual e or μ leptons is measured relative to their transverse momentum p_{T}^{ℓ}, by summing over charged and neutral particles in a cone $\Delta R = \sqrt{(\eta^{\ell} - \eta^{i})^2 + (\phi^{\ell} - \phi^{i})^2} < 0.4$ around the lepton direction at the interaction vertex:

$$R_{\mathrm{Iso}}^{\ell} \equiv \left(\sum p_{\mathrm{T}}^{\mathrm{charged}} + \mathrm{MAX}\left[0, \sum p_{\mathrm{T}}^{\mathrm{neutral}} + \sum {p_{\mathrm{T}}}^{\gamma} - \rho \times A_{\mathrm{eff}}, \right] \right) / p_{\mathrm{T}}^{\ell} \ .$$

The $\sum p_{\mathrm{T}}^{\mathrm{charged}}$ is the scalar sum of the transverse momenta of charged hadrons originating from the primary vertex. The primary vertex is chosen as the vertex with the highest sum of p_{T}^2 of its constituent tracks. The $\sum p_{\mathrm{T}}^{\mathrm{neutral}}$ and $\sum p_{\mathrm{T}}{}^{\gamma}$ are the scalar sums of the transverse momenta for neutral hadrons and photons, respectively. The latter excludes photons that are candidates for final-state radiation (FSR) from the lepton (see below). Vetoes are used to account for the small differences between reconstructed electron candidates and those identified from the PF algorithm in the isolation evaluation. The average transverse momentum flow density ρ is caculated in each event using a "jet area" technique [28]. It is defined as the median of the distribution for the neutral particles around all jets (any PF jet in the event having $p_{\mathrm{T}}^{\mathrm{jet}} > 3$ GeV). The effective area A_{eff} is the geometric area of the isolation cone times a correction factor which accounts for residual dependence of the isolation on pile-up as a function of η. The electrons or muons are considered isolated in the $\mathrm{H} \to 4\ell$ analysis if $R_{\mathrm{Iso}}^{\ell} < 0.4$. Tighter isolation requirements are imposed for leptons in the $\mathrm{H} \to 2\ell 2\tau$ analysis depending on the assignment to either the $\mathrm{Z} \to \ell^+\ell^-$, for which $R_{\mathrm{Iso}}^{\ell} < 0.25$ is required, or to $\mathrm{Z} \to \tau_{\ell} + \tau_{\mathrm{h}}$, for which $R_{\mathrm{Iso}}^{\ell} < 0.1$ is required for $\tau_{\mathrm{e}}\tau_{\mathrm{h}}$ and 0.15 for $\tau_{\mu}\tau_{\mathrm{h}}$ final states respectively.

The electron or muon pairs from Z decays should originate from the primary vertex. This is ensured by requiring that the significance of the impact parameter to the event vertex, $\mathrm{SIP}_{3\mathrm{D}}$, satisfies $\mathrm{SIP}_{3\mathrm{D}} = |\frac{\mathrm{IP}}{\sigma_{\mathrm{IP}}}| < 4$ for each lepton. The IP is the lepton impact parameter in three dimensions at the point of closest approach with respect to the primary interaction vertex, and σ_{IP} is its associated uncertainty.

The efficiencies for the product of reconstruction, identification, and isolation of primary e or μ leptons are measured in data, using a tag-and-probe technique [29] based on an inclusive sample of Z events. The measurements are performed in several bins of p_{T}^{ℓ} and $|\eta|$. The efficiencies for selecting electrons in the ECAL barrel (endcaps) varies from about 70% (60%) for $7 < p_{\mathrm{T}}^{\mathrm{e}} < 10\,\mathrm{GeV}$ to 85% (77%) at $p_{\mathrm{T}}^{\mathrm{e}} \simeq 10\,\mathrm{GeV}$, and reaches 95% (89%) for $p_{\mathrm{T}}^{\mathrm{e}} \geq 20\,\mathrm{GeV}$. It is about 85% in the transition region, $1.44 < |\eta| < 1.57$, between the ECAL barrel and endcaps, averaging over the whole p_{T} range. The muons are reconstructed and identified with efficiencies above ~98% in the full $|\eta^{\mu}| < 2.4$ range. The efficiency of the τ_h reconstruction is aproximately 50%. The performance for the tau lepton identification is discussed in Ref. [27].

Photons reconstructed within $|\eta^{\gamma}| < 2.4$ are possible FSR candidates. To be accepted as FSR, a reconstructed photon must either have a transverse momentum $p_{\mathrm{T}}^{\gamma} > 2\,\mathrm{GeV}$ and be found within $\Delta R < 0.07$ from a selected lepton candidate, or have $p_{\mathrm{T}}^{\gamma} > 4\,\mathrm{GeV}$ and be found isolated within $0.07 < \Delta R < 0.5$ around a selected lepton candidate. The photon isolation observable $R_{\mathrm{Iso}}^{\gamma}$ is the sum, divided by p_{T}^{γ}, of the transverse momenta of charged hadrons, other photons and neutral hadrons identified by the PF reconstruction in a cone of size $\Delta R = 0.3$ around the candidate photon direction. Isolated photons must satisfy $R_{\mathrm{Iso}}^{\gamma} < 1$.

The performance of the FSR selection algorithm has been measured using MC simulation samples, and the rate was verified with single-Z and data events. The photons within the acceptance for the FSR selection are measured with an efficiency of $\simeq$ 50% and with a mean purity of 80%. FSR photons are selected in 5% of single-Z events with muon pairs, and 0.5% of single-Z events with electron pairs. A gain of $\simeq$ 3% (2%, 1%) in efficiency is expected for the selection of $\mathrm{H} \to 4\mu$ (2e2μ, 4e) events in this analysis.

3 Datasets

Collision events are selected by the trigger system that requires the presence of a pair of electrons or a pair of muons, or a triplet of electrons. The usage of triple electrons triggers adds 1

to 3% signal efficiency in the 4e channel compared to the analysis presented in [10]. A trigger requiring an electron and a muon is also used for the 2012 data. The minimal momenta of the first and second lepton are 17 and 8 GeV, respectively, for the double lepton triggers, while they are 15, 8 and 5 GeV for the triple electron trigger. The trigger efficiency within the acceptance of this analysis is greater than 98% for a Higgs boson signal with $m_{\mathrm{H}} > 120\,\mathrm{GeV}$ in the 4ℓ channels, and for $m_H > 200\,\mathrm{GeV}$ in the $2\ell 2\tau$ channels.

Monte Carlo (MC) samples for the SM Higgs boson signal and for background processes are used to optimize the event selection and to evaluate the acceptance and systematic uncertainties. The Higgs boson signals from gluon-fusion ($gg \to H$), and vector-boson fusion ($qq \to qqH$), are generated with POWHEG [30] at next-to-leading order (NLO) and a dedicated generator from Ref. [31] for angular correlations. At low mass, the analysis is carried out in the framework of the narrow-width approximation, describing the Higgs lineshape with a Breit-Wigner distribution. This approximation breaks down at high mass (typically $m_H > 400\,\mathrm{GeV}$) due to the very large Higgs width ($\Gamma_{\mathrm{H}} > 70\,\mathrm{GeV}$). The lineshape is therefore corrected to match the results presented in [32–34] where the complex-pole scheme approach is described. Moreover, the interference between the Higgs boson signal produced by gluon-fusion and the background from $gg \to ZZ$ is taken into account, as suggested in Ref. [35]. The theoretical uncertainty on the shape of the resonance due to missing higher order (NLO) in the interference between background and signal is included, as well as the uncertainties due to electroweak corrections [33, 35, 36]. Additional samples of WH, ZH, and $t\bar{t}H$ events are generated with PYTHIA [37]. Events at generator level are reweighted according to the total cross section $\sigma(pp \to H)$, which contains contributions from gluon fusion up to next-to-next-to-leading order (NNLO) and next-to-next-to-leading log taken from Refs. [38–49] and from the weak-boson fusion contribution computed at NNLO in Refs. [41, 50–54]. The total cross section is scaled by the branching fraction $\mathcal{B}(H \to 4\ell)$ calculated with PROPHECY4F, which includes NLO QCD and electroweak corrections and all interference effects at NLO [41, 55–58], in particular effects specific to the 4e and 4μ channels. The SM background contribution from ZZ production via $q\bar{q}$ is generated at NLO with POWHEG, while other diboson processes (WW, WZ) are generated with MADGRAPH [59] with cross sections rescaled to NLO predictions. The $gg \to ZZ$ contribution is generated with GG2ZZ [60]. The $Zb\bar{b}$, $Zc\bar{c}$, $Z\gamma$, and $Z +$ light jets samples are generated with MADGRAPH, as contributions to inclusive Z production, with cross sections rescaled to NNLO prediction for inclusive Z production. The $t\bar{t}$ events are generated at NLO with POWHEG. The generation takes into account the internal initial-state and final-state radiation effects which can lead to the presence of additional hard photons in an event. For leading-order generators, the default set of parton distribution functions (PDF) used to produce these samples is CTEQ6L [61], while CT10 [62] is used for NLO generators. All generated samples are interfaced with PYTHIA. All events are processed through a detailed simulation of the CMS detector based on GEANT4 [63] and are reconstructed with the same algorithms that are used for data. The simulations include pileup interactions matching the distribution of the number of such interactions observed in data.

4 Event selection and kinematics

The event selection is built to give a mutually exclusive set of signal candidates in the $H \to 4\ell$ and $H \to 2\ell 2\tau$ channels.

The signal candidates in the 4ℓ analysis are first selected. The selection uses well identified and isolated primary leptons. The lepton isolation requirements suppress the Z+jet, $Zb\bar{b}$ and $t\bar{t}$ backgrounds. The requirement on the significance of the impact parameter to the event vertex

$SIP_{3D} < 4$ further suppresses the $Zb\bar{b}$ and $t\bar{t}$ backgrounds. When building the Z candidates, only the FSR photons associated with the closest lepton and which make the "dressed" lepton-pair mass closer to the nominal Z mass are kept, with a maximum mass $m_{\ell\ell\gamma} < 100\,\text{GeV}$. In the following, the presence of the photons in the 4ℓ kinematics is implicit. We require a Z candidate formed with a pair of leptons of the same flavour and opposite charge ($\ell^+\ell^-$). The pair with an invariant mass closest to the nominal Z mass is denoted m_{Z_1} and retained if it satisfies $40 < m_{Z_1} < 120\,\text{GeV}$. We then consider all remaining leptons and require a second pair of $\ell^+\ell^-$, with mass denoted m_{Z_2}, to satisfy $12 < m_{Z_2} < 120\,\text{GeV}$. The 12 GeV cut provides an optimal sensitivity for a Higgs boson mass hypothesis in the range $110 < m_H < 160\,\text{GeV}$. If more than one Z_2 candidate satisfies all criteria, the ambiguity is resolved by choosing the leptons of highest p_T. Among the four selected leptons forming Z_1 and the Z_2, at least one should have $p_T > 20\,\text{GeV}$ and another one have $p_T > 10\,\text{GeV}$. These p_T thresholds ensure that the selected events have leptons on the high-efficiency plateau for the trigger. To further protect against leptons originating from hadron decays in jet fragmentation or from the decay of low-mass hadronic resonances, we require that any opposite-charge pair of leptons chosen among the four selected leptons (irrespective of flavour) satisfy $m_{\ell\ell'} > 4\,\text{GeV}$. The phase space for the search of the SM Higgs boson is defined by restricting the mass range to $m_{4\ell} > 100$ GeV. A higher minimal threshold on m_{Z_1} and m_{Z_2} could be used for higher m_H values but only with marginal improvement of the sensitivity.

For the search in the $2\ell2\tau$ final state, events are required to have one $Z_1 \to \ell^+\ell^-$ candidate with one lepton at $p_T > 20\,\text{GeV}$ and the other at $p_T > 10\,\text{GeV}$, and a $Z_2 \to \tau^+\tau^-$, with τ decaying into μ, e or τ_h. The leptons from the τ leptonic decays are required to have $p_T^\ell > 10\,\text{GeV}$. The τ_h are required to have $p_T^{\tau_h} > 20\,\text{GeV}$. The FSR recovery is not applied for the $2\ell2\tau$ final state. The invariant mass of the reconstructed Z_1 is required to satisfy $60 < m_{\ell\ell} < 120\,\text{GeV}$, and that of the Z_2 to satisfy $m_{\tau\tau} < 90\,\text{GeV}$. At low $m_{\tau\tau}$, the Z_2 is restricted by the selection requirements on the p_T of the leptons. Thus, the $2\ell2\tau$ final states contribute only to the "high-mass" part of the analysis ($m_{\ell2\tau} > 180$ GeV).

The event yields are found to be in good agreement with the MC background expectation at each step of event selection.

Kinematics of the Higgs or exotic boson decay to ZZ final state has been extensively studied in the literature [31, 64–76]. Since the Higgs boson is spinless, the angular distribution of its decay products is independent of the production mechanism. Five angles $\vec{\Omega} = (\theta^*, \Phi_1, \theta_1, \theta_2, \Phi)$, defined in Ref. [31], and the invariant masses of the lepton pairs, m_{Z_1} and m_{Z_2}, fully describe the kinematics of the $H \to ZZ \to 4\ell$ process at a given mass of the four-lepton system in their centre-of-mass frame. These observables provide significant discriminating power between signal and background.

We use a matrix element likelihood analysis (MELA). We construct a kinematic discriminant (K_D) based on the probability ratio of the signal and background hypotheses, MELA $K_D = \mathcal{P}_{sig}/(\mathcal{P}_{sig} + \mathcal{P}_{bkg})$, as described in Refs. [31, 75]. The likelihood ratio is defined for each value of $m_{4\ell}$. The signal and $q\bar{q} \to ZZ/Z\gamma^*$ background analytical parametrisations are taken from Refs. [31, 75] and Refs. [74, 76], respectively. The analytical parameterization for background at the low mass range has been an improvement in the discriminant since Ref. [10]. This approach has also been validated with independent implementations of the kinematic discriminants either using directly the matrix element from JHUGen [31, 75], MCFM [77–79], MADGRAPH [59], or CalcHEP [80], standalone or within the generalized MEKD framework [81], or using the Boosted Decision Trees multivariate classification technique trained with the MC samples. Similar performance was observed in all these validation tests.

5 Background control and systematics

We rely on MC simulation to evaluate the local density ($\Delta N/\Delta m_{4\ell}$) of events expected as a function of the mass $m_{4\ell}$ from the ZZ background. Following the prescription used in the previous analysis, the cross section for ZZ production at NLO is calculated with MCFM [77–79]. This includes the dominant process of $q\bar{q}$ annihilation, as well as gluon fusion. The theoretical uncertainties are computed as a function of $m_{4\ell}$, varying both the QCD renormalisation and factorization scales and the PDF set, following the PDF4LHC recommendations [82–86]. The uncertainties for the QCD and PDF scales for each final state are on average 8%. The number of predicted $ZZ \to 4\ell$ events and their uncertainties after the signal selection are given in Table 1.

To estimate the reducible ($Zb\bar{b}$, $t\bar{t}$) and instrumental (Z + light jets, WZ + jets) backgrounds, a Z_1+X background control region, well separated from the signal region, is defined. In addition, a sample $Z_1 + \ell_{\text{reco}}$, with at least one reconstructed lepton object, is defined for the measurement of the lepton misidentification probability — the probability for a reconstructed object to pass the isolation and identification requirements. The contamination from WZ in these events is suppressed by requiring the imbalance of the measured energy deposition in the transverse plane to be below 25 GeV. The lepton misidentification probability is compared, and found compatible, with the one derived from MC simulation. The event rates measured in the background control region are extrapolated to the signal region.

Two different approaches are used. Both start by relaxing the isolation and identification criteria for two additional reconstructed lepton objects. A first approach follows from previous CMS analysis [12]. The additional pair of leptons is required to have the same charge (to avoid signal contamination) and same flavour ($e^{\pm}e^{\pm}$, $\mu^{\pm}\mu^{\pm}$), a reconstructed invariant mass $m_{Z_2} > 12$ GeV, and $m_{4\ell} > 100$ GeV. The expected number of Z+X background events in the signal region is obtained by taking into account the lepton misidentification probability for each of the two additional leptons. The second method, used also for $\tau\tau$ final states, employs the control region with two opposite-sign leptons failing the isolation and identification criteria. In addition, a control region with three passing and one failing lepton is also used to account for contributions from backgrounds with three prompt leptons and one misidentified lepton. The validity of the two methods is assessed with closure tests in the simulation and checks with data on samples using relaxed charge and flavor requirements. Comparable background counts in the signal region are found within uncertainties from both methods. An envelope comprising these results is used as the final estimate in Table 1.

Systematic uncertainties are evaluated from data for trigger (1.5%), and combined lepton reconstruction, identification and isolation efficiencies (varying from 1.2% to 3.8% in the 4μ channel and from 5.5% to 11% in $4e$ channel, depending on the considered mass). The uncertainty associated with τ_h identification and isolation is 6%. Uncertainties on τ_h energy scale (3%) contribute to variation in the shape of the mass spectrum. Samples of $Z \to \ell\ell$, $\Upsilon \to \ell\ell$ and $J/\psi \to \ell\ell$ are used to validate the absolute momentum scale and resolution. Systematic uncertainties on per-lepton energy-momentum calibration are estimated to be 0.1% for muons. For electrons, a p_T dependance is observed, the largest error being 0.4% (1%) in the barrel (endcaps). This translates into uncertainties of 0.1% and 0.2% in the 4μ and 4e reconstructed masses, respectively. The effect of the energy resolution uncertainties is taken into account by introducing a 20% uncertainty on the simulated width of the signal mass peak. Additional systematic uncertainties arise from the limited statistical precision in the reducible background control regions as well as the difference in background composition between the control regions and the sample on which the lepton misidentification probability is derived. Each of the methods described above is assigned an uncertainty of about 50%. The total uncertainty on

the reducible background estimate for the $2\ell2\tau$ final state is approximately 30%. All reducible and instrumental background sources are derived from control regions, and the comparison of data with the background expectation in the signal region is independent of the uncertainty on the LHC integrated luminosity of the data sample. This uncertainty (2.2% at 7 TeV, 4.4% at 8 TeV) [87] enters the evaluation of the ZZ background and in the calculation of the cross section limit through the normalisation of the signal. Systematic uncertainties on the Higgs boson cross section (17 – 20%) and branching fraction (2%) are taken from Ref. [41].

6 Results

The reconstructed four-lepton invariant-mass distributions for the 4ℓ, combining the 4e, 4μ, and $2e2\mu$ channels, are shown in Fig. 1 (left) and compared with the expectation from SM background processes. The observed distribution is in good agreement with the expectation. The

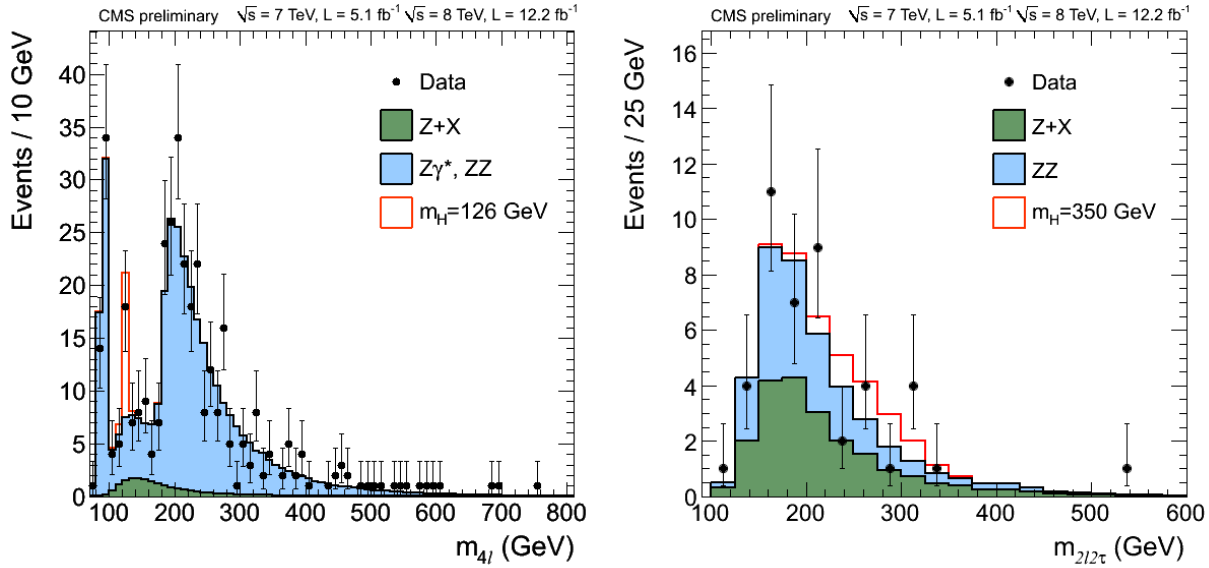

Figure 1: Distribution of the four-lepton reconstructed mass in full mass range for the sum of the 4e, 4μ, and $2e2\mu$ channels (left), and for the sum over all $\ell^+\ell^-\tau^+\tau^-$ channels (right). Points represent the data, shaded histograms represent the background and unshaded histogram the signal expectations. The expected distributions are presented as stacked histograms. The measurements are presented for the sum of the data collected at $\sqrt{s} = 7\,\text{TeV}$ and $\sqrt{s} = 8\,\text{TeV}$. No event is observed for $m_{4\ell} > 800$ GeV or $m_{2\ell2\tau} > 600$ GeV.

peak of the $Z \to 4\ell$ candle around $m_{4\ell} = m_Z$ is observed as expected. The measured distribution at higher mass is dominated by the irreducible ZZ background. A clear peak around $m_{4\ell} = 126$ GeV is seen, confirming the results reported in [10]. The reconstructed visible mass distributions for the $2\ell2\tau$ selection, combining all the $\ell^+\ell^-\tau^+\tau^-$ final states, are shown in Fig. 1 (right) and compared to SM background expectation. The background shapes are taken from MC simulation and the rates are normalised to the values obtained using a method based on data. The measured distribution is well described by the SM background expectation.

The number of candidates observed as well as the estimated background are reported in Table 1, for the selection in the full mass measurement range for the SM-like Higgs boson search, $100 < m_{4\ell}, m_{2\ell2\tau} < 1000\,\text{GeV}$. The expected number of signal events is also given for several

SM-like Higgs boson mass hypotheses. The observed event rates for the various channels are compatible with SM background expectation.

Table 1: The number of event candidates observed, compared to the mean expected background and signal rates for each final state. For the Z +X background, the estimations are based on data. The results are given integrated over the full mass measurement range for the SM-like Higgs boson search from 100 to 1000 GeV and for 2011 and 2012 data combined.

Channel	4e	4μ	$2e2\mu$	$2\ell2\tau$
ZZ background	53.0 $\pm$6.3	82.7 $\pm$8.9	131.1 $\pm$14.3	19.0 $\pm$2.3
Z+ X	7.6 $^{+6.9}_{-5.2}$	2.9 $^{+2.2}_{-1.6}$	10.1 $^{+9.9}_{-6.5}$	20.4 $\pm$6.2
All background expected	60.7 $^{+9.3}_{-8.2}$	85.6 $^{+9.2}_{-9.1}$	141.3 $^{+17.3}_{-15.7}$	39.4 $\pm$6.6
m_H = 125 GeV	2.4 $\pm$0.4	4.6 $\pm$0.5	6.0 $\pm$0.7	–
m_H = 126 GeV	2.7 $\pm$0.4	5.1 $\pm$0.6	6.6 $\pm$0.8	–
m_H = 200 GeV	15.5 $\pm$1.9	23.1 $\pm$2.6	38.5 $\pm$4.3	5.6 $\pm$0.6
m_H = 350 GeV	9.5 $\pm$1.2	13.6 $\pm$1.5	23.2 $\pm$2.7	5.7 $\pm$0.6
m_H = 500 GeV	3.3 $\pm$0.4	4.7 $\pm$0.6	8.1 $\pm$0.9	2.8 $\pm$0.3
m_H = 800 GeV	0.5 $\pm$0.1	0.6 $\pm$0.1	1.1 $\pm$0.1	0.3 $\pm$0.1
Observed	59	95	162	45

The distributions of the MELA K_D versus the four-lepton reconstructed mass $m_{4\ell}$ is shown for the selected events and compared to SM background expectation in Fig. 2. The distribution of

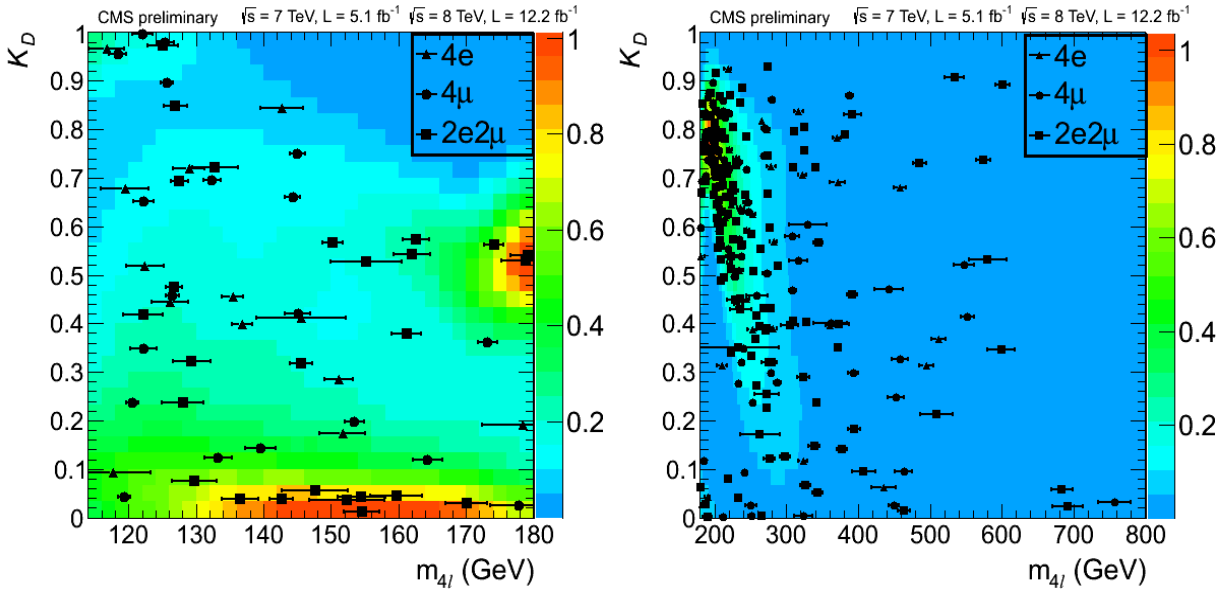

Figure 2: Distribution of the MELA K_D versus the four-lepton reconstructed mass $m_{4\ell}$ in the low-mass (left) and high-mass (right) regions. The contours represent the expected relative density of background events. The points show data with measured invariant mass uncertainties. No event is observed for $m_{4\ell} > 800$ GeV.

events in the $(m_{4\ell}, K_D)$ plane is seen to agree well with the SM expectation in the high mass range (Fig. 2, right).

The measured distributions are compared with the expectation from SM background processes, and exclusion limits at 95% CL on the ratio of the production cross section for the SM-like Higgs boson to the SM expectation are derived. For this, the $(m_{4\ell}, K_D)$ distributions of the selected events are split into six categories based on three final states and two running periods (7 and 8 TeV). These events are examined for 187 hypothetical SM-like Higgs boson masses in a range between 110 GeV and 1000 GeV, where the mass steps are optimized to account for the expected width and resolution for the measurement of m_{H} [88]. For each mass hypothesis, we perform a simultaneous likelihood fit of the six two-dimensional $(m_{4\ell}, K_D)$ distributions using the statistical approaches discussed in Ref. [88]. As a cross-check, we have also studied one-dimensional $m_{4\ell}$ distributions and found consistent, but systematically higher expected limits. We adopt the modified frequentist construction $\mathrm{CL_s}$ [88–90] as the primary method for reporting limits. As a complementary method to the frequentist paradigm, we use the Bayesian approach [91] and find consistent results.

The probability distribution of $\mathcal{P}(m_{4\ell})$ for the background is parametrised with empirical functions using MC simulation for ZZ background and data control regions for Z + X background. The reconstructed signal $m_{4\ell}$ distributions are described with a relativistic Breit-Wigner parametrization convoluted with a double-sided Crystal-Ball function [92]. The correlated two-dimensional $(m_{4\ell}, K_D)$ distribution is described by the one-dimensional probability distribution $\mathcal{P}(m_{4\ell})$ multiplied by a two-dimensional template distribution normalised in the K_D dimension. This template distribution is obtained from simulation for both signal and ZZ background, accounting for interference effects of identical leptons in the final state. It has been verified that the K_D distribution of the Z + X background is consistent with that of the ZZ background, and any potential small difference is accounted for in the systematic uncertainties.

For the $2\ell 2\tau$ channels, signal and background shape templates are taken from simulation, with the background yields normalised to the data-driven yields described above. Shape variations due to τ energy scale uncertainties are accounted for by vertical template morphing. Due to the limited number of simulated events, the reducible background shape was taken with relaxed isolation requirements on the second Z boson. Normalizations for backgrounds vary within the uncertainties. All systematic uncertainties are included in the likelihood with log-normal distributions.

The upper limits obtained from the combination of the 4ℓ and $2\ell 2\tau$ channels are shown in Fig. 3 (left). The SM-like Higgs boson is excluded by the four-lepton channels at 95% CL in the ranges 113–116 GeV and 129–720 GeV. The upper limits in the low-mass region are given in Fig. 4 (left). The local p-values, representing the significance of local excesses relative to the background expectation, are shown for the full mass range as a function of m_{H} in Fig. 3 (right) and for the low-mass region in Fig. 4 (right). The minimum of the local p-value is reached at low mass around $m_{4\ell} = 125.9$ GeV, near the mass of the new boson [10], and corresponds to a local significance of 4.5σ.

Table 2 reports the number of observed and predicted events in the mass region near the signal, from 110 to 160 GeV, where the background is expected to be relatively flat.

The distribution of the four-lepton reconstructed mass for the sum of the 4e, 4μ, and $2\mathrm{e}2\mu$ channels, and the distribution of the MELA K_D versus the four-lepton reconstructed mass $m_{4\ell}$ are shown in Fig. 5 in the low mass range. A signal-like clustering of events is apparent at high values of K_D, as seen in Fig. 6 (left), and for $m_{\mathrm{H}} \approx 126$ GeV. As an illustration, the reconstructed four-lepton invariant-mass distribution for the 4ℓ is shown in Fig. 6 for events with $K_D > 0.5$.

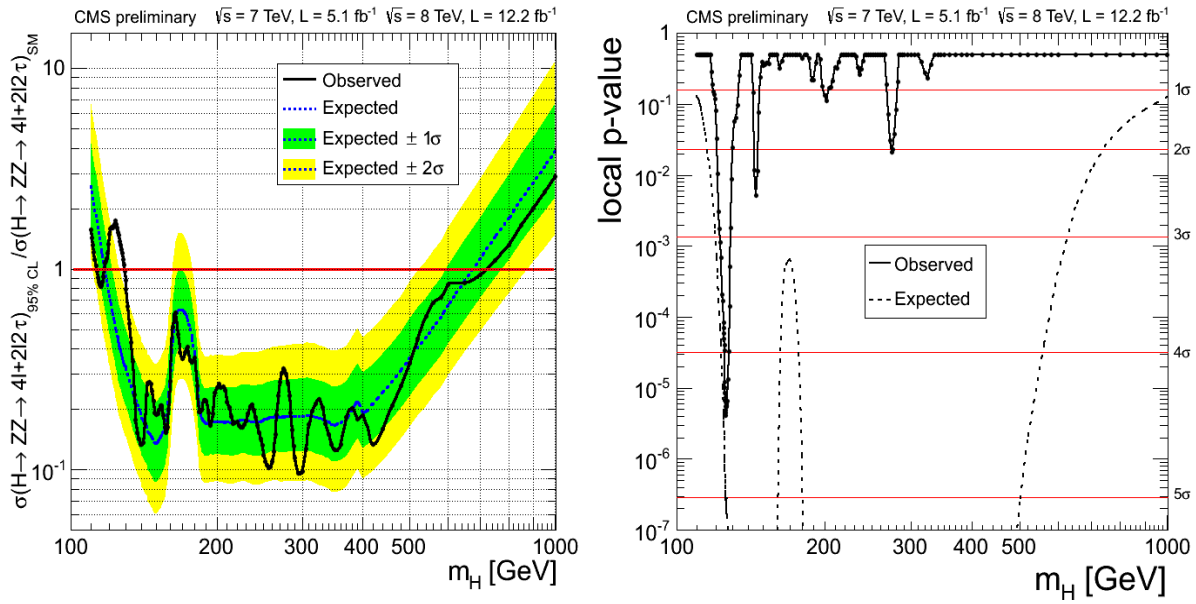

Figure 3: Observed and expected 95% CL upper limit (left) on the ratio of the production cross section to the SM expectation. The 68% and 95% ranges of expectation for the background-only model are also shown with green and yellow bands, respectively. Significance of the local excess (right) with respect to the standard model background expectation as a function of the Higgs boson mass in the full interpretation mass range 110-1000 GeV.

The signal strength μ, relative to the expectation for the SM Higgs boson, is measured to be $\mu = 0.80^{+0.35}_{-0.28}$ at 126 GeV. The local significance of 3.1σ is reached in the 1D fit without the MELA K_D. The average expected significance for a SM Higgs boson at this mass is 5.0σ and 4.3σ for the 2D and 1D fits, respectively. Using simulation it was found that the MELA K_D distribution for signal at a mass around $m_H = 126$ GeV is similar for a scalar, pseudo-scalar, or a spin-two resonance with the minimal couplings [31]. Therefore the analysis presented is nearly model-indepedent in the low-mass region.

In the following, we discuss in more detail measurements of the new boson properties.

Table 2: The number of event candidates observed, compared to the mean expected background and signal rates for each final state. For the Z +X background, the estimations are based on data. The results are given integrated in the mass range from 110 to 160 GeV.

Channel	4e	4μ	2e2μ	4ℓ
ZZ background	4.7 $\pm$0.6	9.6 $\pm$1.0	12.5 $\pm$1.4	26.8 $\pm$1.8
Z+ X	$3.4^{+3.0}_{-2.3}$	$1.6^{+1.2}_{-0.9}$	$5.6^{+5.4}_{-3.6}$	$10.6^{+5.3}_{-4.4}$
All backgrounds	$8.0^{+3.1}_{-2.3}$	$11.2^{+1.6}_{-1.4}$	$18.1^{+5.6}_{-3.8}$	$37.3^{+6.6}_{-4.7}$
m_H = 125 GeV	2.4 $\pm$0.4	4.6 $\pm$0.5	5.9 $\pm$0.7	12.9 $\pm$0.9
m_H = 126 GeV	2.7 $\pm$0.4	5.1 $\pm$0.6	6.6 $\pm$0.8	14.4 $\pm$1.1
Observed	12	16	19	47

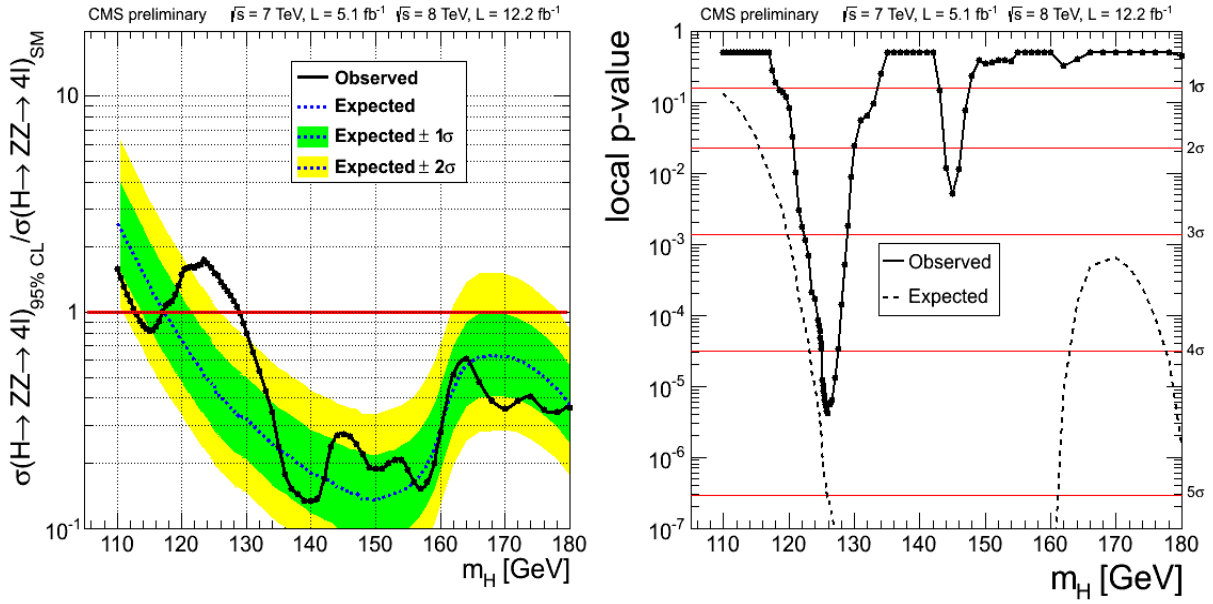

Figure 4: Observed and expected 95% CL upper limit (left) on the ratio of the production cross section to the SM expectation, in the low-mass region. The 68% and 95% ranges of expectation for the background-only model are also shown with green and yellow bands, respectively. Significance of the local excess (right) with respect to the standard model background expectation as a function of the Higgs boson mass. The results are shown for the full data sample in the low-mass region only.

6.1 Mass measurement

The mass measurement of the new resonance is performed with a three-dimensional fit using for each event the four-lepton invariant mass, the associated per-event mass error, and the kinematic discriminant. Per-event errors on the 4-lepton invariant mass are calculated from the individual lepton momentum errors. Individual lepton momentum errors are computed for muons using the full error matrix, as obtained from the muon track fit, and for electrons using the estimated momentum error, as obtained from the combination of the ECAL and tracker measurements. The shape of the per-event error distributions for the signal and the ZZ background are extracted from the MC simulation and are cross-checked with data in the control region for the ZZ background. The corresponding shape for the reducible background is extracted from the control regions in data. The correlation between per-event errors and the kinematical discriminant can be neglected, as was verified with MC simulation. The systematic uncertainties are evaluated by making comparisons between data and MC samples of $Z \to ee$ and $Z \to \mu\mu$, and using simulated signal samples. Uncertainty of 20% are assumed on the mass resolution for all channels. Uncertainties of 0.1%, 0.2%, and 0.2% are assumed on the mass scale for the 4μ, $2e2\mu$, and $4e$ channels respectively.

Figure 7 shows the two-dimensional 68% CL regions for the signal strength μ, relative to the expectation for the Standard Model Higgs boson, versus m_{H}. A simultaneous fit of the mass and of signal strength gives $m_{\mathrm{H}} = 126.2 \pm 0.6$ (stat) ± 0.2 (syst) GeV.

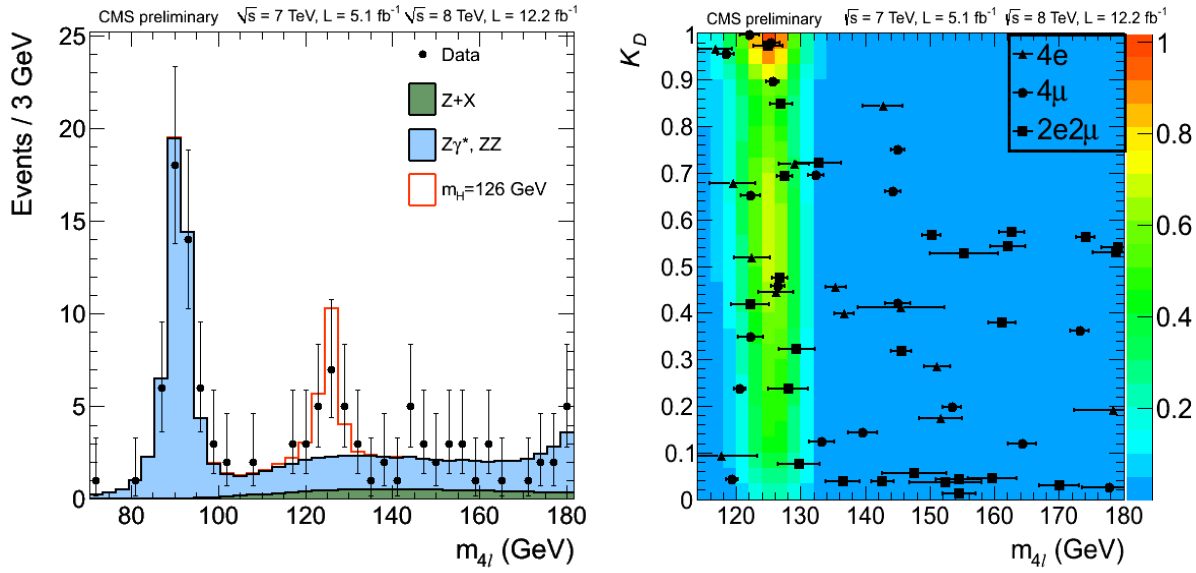

Figure 5: Distribution of the four-lepton reconstructed mass for the sum of the 4e, 4μ, and 2e2μ channels (left). Points represent the data, shaded histograms represent the background and unshaded histogram the signal expectations. Distribution of the MELA K_D versus the four-lepton reconstructed mass $m_{4\ell}$ (right) with contours shown for expected relative density of signal events for hypothesis $m_H = 126$ GeV. The points show data with measured invariant mass uncertainties.

6.2 Parity measurement

It is crucial to determine the spin and quantum numbers of the new boson. Kinematics of the Higgs or exotic boson decay to ZZ final state has been extensively studied in the literature [31, 64–76]. The full-case study has been presented in Refs. [31, 75]. Here we follow the MELA methodology, where instead of signal-to-background probability ratio we construct probability ratio for two signal hypotheses. The discriminant for signal hypothesis testing is constructed as follows

$$\mathcal{D}_{J^P} = \frac{\mathcal{P}_{\rm SM}}{\mathcal{P}_{\rm SM} + \mathcal{P}_{J^P}} = \left[1 + \frac{\mathcal{P}_{J^P}(m_1, m_2, \vec{\Omega}|m_{4\ell})}{\mathcal{P}_{\rm SM}(m_1, m_2, \vec{\Omega}|m_{4\ell})}\right]^{-1}, \tag{1}$$

where $\mathcal{P}_{\rm SM}$ is the probability distribution for the SM Higgs boson hypothesis, $\mathcal{P}_{J^P}$ is the probability for an alternative model.

We consider the pure pseudo-scalar state $J^P = 0^-$ as an alternative hypothesis. The most general decay amplitude for a spin-zero boson can be defined as

$$A = v^{-1}\epsilon_1^{*\mu}\epsilon_2^{*\nu}\left(a_1 g_{\mu\nu} m_H^2 + a_2\, q_\mu q_\nu + a_3 \epsilon_{\mu\nu\alpha\beta}\, q_1^\alpha q_2^\beta\right) = A_1 + A_2 + A_3\,, \tag{2}$$

where ϵ_i are the Z boson polarization vectors, q_i are their momenta, and $q = q_1 + q_2$ is the four-momentum of the spin-zero boson. The SM Higgs boson decay is dominated by the A_1 amplitude, while the $J^P = 0^-$ state decay is expected to be dominated by the A_3 amplitude. The $\mathcal{D}_{0^-}$ discriminant is therefore optimal for discrimination between the $|A_1|^2$ and $|A_3|^2$ amplitude contributions, while we find their potential interference to have negligible

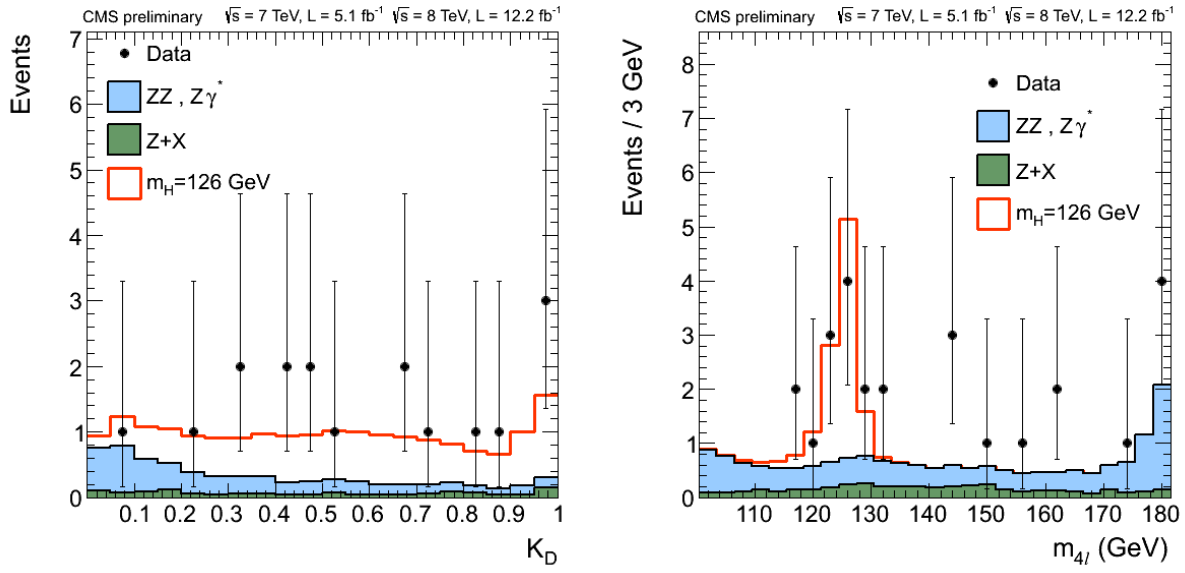

Figure 6: Distribution of the MELA kinematic discriminant for events in the mass region $121.5 < m_{4\ell} < 130.5\,\text{GeV}$ (left). Distribution of the four-lepton reconstructed mass for the sum of the 4e, 4μ, and $2e2\mu$ channels for events with a value $K_D > 0.5$ of the MELA kinematic discriminant (right). Points represent the data, shaded histograms represent the background and unshaded histogram the signal expectations. The measurements are presented for the sum of the data collected at $\sqrt{s} = 7\,\text{TeV}$ and $\sqrt{s} = 8\,\text{TeV}$.

effect on the discriminant distribution or the overall yield of events. We define the parameter $f_{a3} = |A_3|^2/(|A_1|^2 + |A_3|^2)$. Here we neglect the $|A_2|^2$ contribution in order to test the presence of the A_3 amplitude, both are expected to be small or negligible in the SM. The presence of both A_3 and A_1 would indicate *CP* violation. This f_{a3} parameter allows us to provide consistency test of the $f_{a3} = 0$ and $f_{a3} = 1$ scenarios, as well as consider contribution of both amplitudes in the decay. However, we would like to stress that f_{a3} is not a parameter which defines the mixture of parity-even and parity-odd states. The latter would require model-dependent interpretation of the f_{a3} measurement.

The statistical analysis remains similar to the Higgs boson search described earlier where we perform the unbinned likelihood fit of the ensemble of selected events, except that instead of the kinematic discriminant for signal-to-background separation, we use the above kinematic discriminant $\mathcal{D}_{J^P}$ for separation between the two signal hypotheses. The second observable combines the $m_{4\ell}$ probability together with the kinematic probability of the angular and mass distribution as used in the KD calculation, $\mathcal{D}_{\text{bkg}} = \mathcal{P}_{\text{sig}}/(\mathcal{P}_{\text{sig}} + \mathcal{P}_{\text{bkg}})$, where probabilities $\mathcal{P}$ also include the $m_{4\ell}$ parameterizations for $m_H = 126\,\text{GeV}$. The analysis of the $\mathcal{D}_{\text{bkg}}$ discriminant is statistically equivalent to the 2D analysis of the $m_{4\ell}$ and KD distributions. The spin-parity hypothesis analysis is a 2D analysis of the $(\mathcal{D}_{\text{bkg}}, \mathcal{D}_{J^P})$ distributions where correlations of observables are included in the probability parameterizations. In the Figure 8 the $\mathcal{D}_{\text{bkg}}$ and $\mathcal{D}_{0^-}$ distributions are shown in the mass range $106 < m_{4\ell} < 141\,\text{GeV}$ used to perform this measurement. The $\mathcal{D}_{\text{bkg}}$ distributions are very similar between the scalar and pseudoscalar hypotheses but differ significantly from background. The $\mathcal{D}_{0^-}$ distributions provide most discrimination between the two signal hypotheses.

Figure 9 (left) shows the distribution of $q = -2\ln(\mathcal{L}_{0^-}/\mathcal{L}_{0^+})$ with generated samples of back-

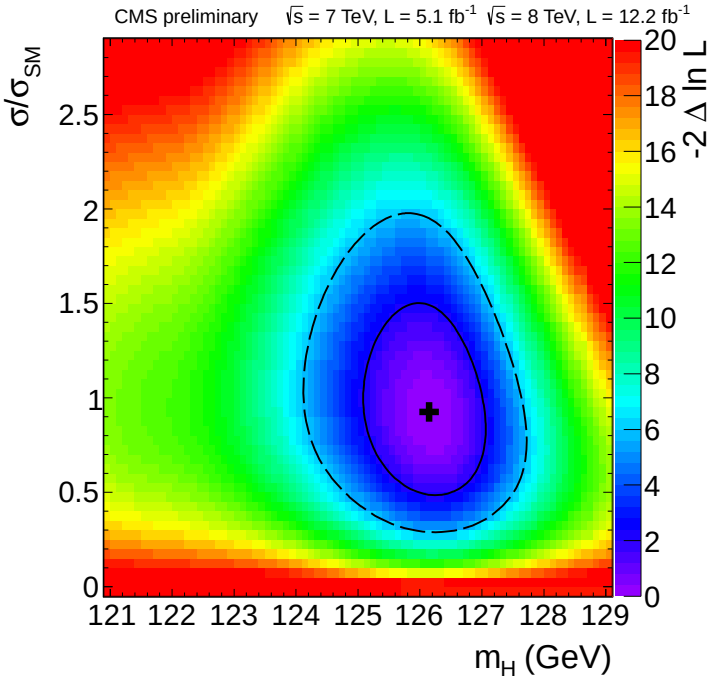

Figure 7: Distribution of $-2\ln\mathcal{L}$ as a function mass m_H and signal strength μ. The central point shows the minimum value of $-2\ln\mathcal{L}$, the solid and dashed contours show 68% and 95% CL contours in two dimensions.

ground and signal of two types, SM 0^+ and 0^-, for $m_H = 126$ GeV. Here the likelihoods, $\mathcal{L}$, are calculated with the signal rates allowed to float independently for each signal type and the nuisance parameters are treated as independent. The expected distributions are generated with signal cross-section equal to that of the SM, which is consistent with observation. We find consistent results when the expected distributions are generated with the measured signal strength. The mean of the expected SM 0^+ distribution is 1.9 standard deviations in the tail of the 0^- distribution, while the mean of the expected 0^- distribution is 2.0 standard deviations in the tail of the 0^+ distribution. The observed value of q, indicated by an arrow in Figure 9 (left), is consistent with expectation, assuming $J^P = 0^-$, within 2.4 standard deviations and consistent with expectation, assuming $J^P = 0^+$, within 0.5 standard deviations. We define a $\mathrm{CL_s}$ criterion as the ratio of the probabilities to observe, under the 0^+ and 0^- hypotheses, a value of the test statistics q equal or larger than the one in the data. The data disfavors the pseudoscalar hypothesis 0^- with a $\mathrm{CL_s}$ value of 2.4%. Figure 9 (right) shows distribution of $-2\ln\mathcal{L}$ as a function of f_{a3} and signal strength, μ. The measurement of the fraction of a *CP*-violating contribution to the decay amplitude expressed through the fraction of the corresponding decay rate is $f_{a3} = 0.00^{+0.31}_{-0.00}$.

7 Summary

In summary, a study of the standard model Higgs boson has been presented in the four-lepton decay modes, $\mathrm{H} \to \mathrm{ZZ} \to 4\ell$ and $\mathrm{H} \to \mathrm{ZZ} \to 2\ell 2\tau$. The mass distributions are measured with four-lepton invariant masses $m_{4\ell}$ or $m_{2\ell 2\tau} > 100\,\mathrm{GeV}$ using 5.1 fb^{-1} at $\sqrt{s} = 7$ TeV and 12.2 fb^{-1} at $\sqrt{s} = 8$ TeV. The measurements are interpreted using for each event the information from the measured four-lepton mass, the mass uncertainty, and a kinematic discriminant. Upper

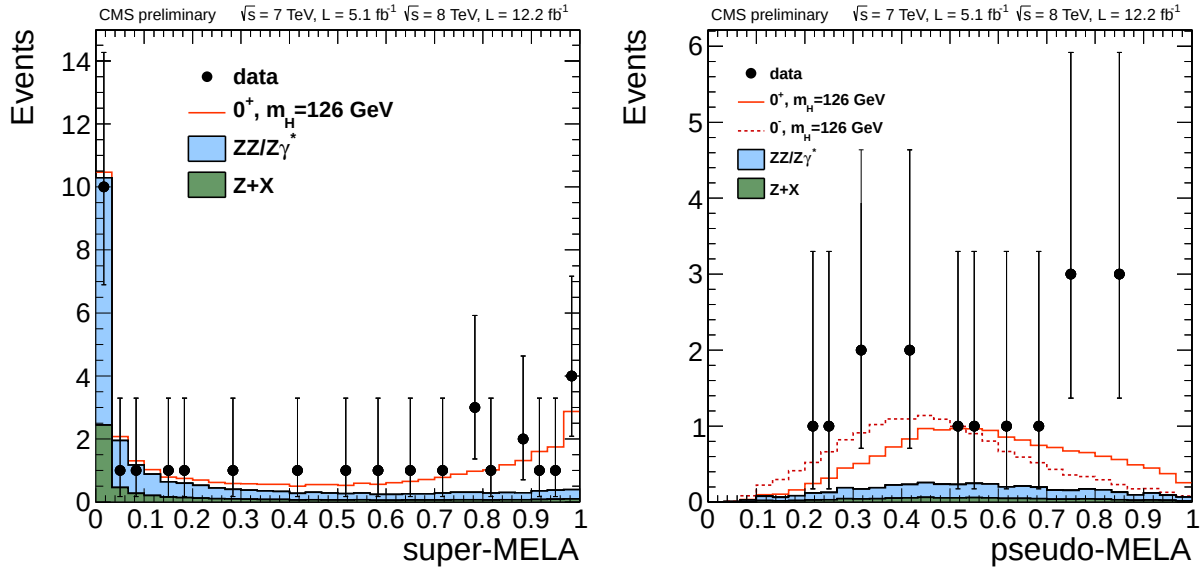

Figure 8: Distribution of $\mathcal{D}_{\rm bkg}$ (left, "super-MELA") and $\mathcal{D}_{0^-}$ (right, "pseudo-MELA") for events in the mass range 106 $<m_{4\ell}<$ 141 GeV. The right plot also requires $\mathcal{D}_{\rm bkg} > 0.5$ to enhance the signal purity. The shaded histograms show background expectation, the open histogram show signal expectation (dashed for pseudoscalar hypothesis), and points show observed data.

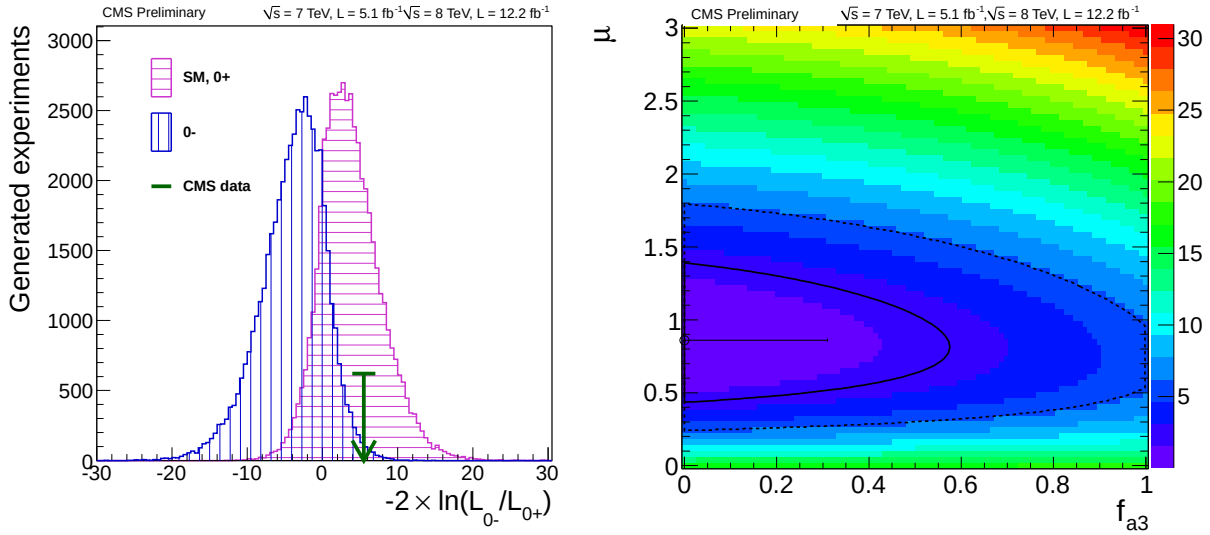

Figure 9: Left: Distribution of $q = -2\ln(\mathcal{L}_{0^-}/\mathcal{L}_{0^+})$ for two signal types (0^+ horizontally hatched histogram, 0^- vertically hatched histogram) for $m_H = 126$ GeV shown with a large number of generated experiments. The arrow indicates the observed value. Right: Distribution of $-2\ln\mathcal{L}$ as a function of f_{a3} and μ. The central point shows the minimum value of $-2\ln\mathcal{L}$, the solid and dashed contours show 68% and 95% CL contours in two dimensions. The one-dimensional 68% CL intervals are shown with the cross.

limits at 95% confidence level exclude the SM-like Higgs boson in the ranges 113–116 GeV

and 129–720 GeV while the expected exclusion range is 118–670 GeV. The new boson recently discovered by the ATLAS and CMS experiments is observed in the 4ℓ channel, with a local significance of 4.5 standard deviations above the expected background. The signal strength μ, relative to the expectation for the standard model Higgs boson, is measured to be $\mu = 0.80^{+0.35}_{-0.28}$ at 126 GeV. A measurement of its mass gives 126.2 ± 0.6 (stat) ± 0.2 (syst) GeV. The hypothesis 0^+ of the standard model for the spin $J = 0$ and parity $P = +1$ quantum numbers is found to be consistent with the observation. Under the assumption that the observed boson has spin zero the data disfavor the pseudoscalar hypothesis 0^- with a CL_s value of 2.4%. The fraction of a CP-violating contribution to the decay amplitude, expressed through the fraction f_{a3} of the corresponding decay rate, is measured to be $f_{a3} = 0.00^{+0.31}_{-0.00}$, and thus consistent with SM expectation.

References

[1] S. L. Glashow, "Partial Symmetries of Weak Interactions", *Nucl. Phys.* **22** (1961) 579, doi:10.1016/0029-5582(61)90469-2.

[2] S. Weinberg, "A Model of Leptons", *Phys. Rev. Lett.* **19** (1967) 1264, doi:10.1103/PhysRevLett.19.1264.

[3] A. Salam, "Weak and electromagnetic interactions", in *Elementary particle physics: relativistic groups and analyticity*, N. Svartholm, ed., p. 367. Almquvist & Wiskell, 1968. Proceedings of the eighth Nobel symposium.

[4] F. Englert and R. Brout, "Broken Symmetry and the Mass of Gauge Vector Mesons", *Phys. Rev. Lett.* **13** (1964) 321, doi:10.1103/PhysRevLett.13.321.

[5] P. W. Higgs, "Broken symmetries, massless particles and gauge fields", *Phys. Lett.* **12** (1964) 132, doi:10.1016/0031-9163(64)91136-9.

[6] P. W. Higgs, "Broken Symmetries and the Masses of Gauge Bosons", *Phys. Rev. Lett.* **13** (1964) 508, doi:10.1103/PhysRevLett.13.508.

[7] G. S. Guralnik, C. R. Hagen, and T. W. B. Kibble, "Global Conservation Laws and Massless Particles", *Phys. Rev. Lett.* **13** (1964) 585, doi:10.1103/PhysRevLett.13.585.

[8] P. W. Higgs, "Spontaneous Symmetry Breakdown without Massless Bosons", *Phys. Rev.* **145** (1966) 1156, doi:10.1103/PhysRev.145.1156.

[9] T. W. B. Kibble, "Symmetry breaking in non-Abelian gauge theories", *Phys. Rev.* **155** (1967) 1554, doi:10.1103/PhysRev.155.1554.

[10] CMS Collaboration, "Observation of a new boson at a mass of 125 GeV with the CMS experiment at the LHC", *Phys. Lett. B* **716** (2012) 30–61, doi:10.1016/j.physletb.2012.08.021, arXiv:1207.7235.

[11] ATLAS Collaboration, "Observation of a new particle in the search for the Standard Model Higgs boson with the ATLAS detector at the LHC", *Phys. Lett. B* **716** (2012) 1–29, doi:10.1016/j.physletb.2012.08.020, arXiv:1207.7214.

[12] CMS Collaboration, "Search for the standard model Higgs boson in the decay channel H to ZZ to 4 leptons in pp collisions at sqrt(s) = 7 TeV", *Phys. Rev. Lett.* **108** (2012) 111804, doi:10.1103/PhysRevLett.108.111804, arXiv:1202.1997.

[13] ATLAS Collaboration, "Search for the Standard Model Higgs boson in the decay channel $H \to \mathrm{ZZ}(*) \to 4\ell$ with 4.8 fb-1 of pp collision data at $\sqrt{s} = 7$ TeV with ATLAS", *Phys. Lett. B* **710** (2012) 383–402, doi:10.1016/j.physletb.2012.03.005, arXiv:1202.1415.

[14] CMS Collaboration, "Search for the standard model Higgs boson in the H to ZZ to ll to $\tau\tau$ decay channel in pp collisions at $\sqrt{s} = 7$ TeV", *JHEP* **1203** (2012) 081, arXiv:1202.3617.

[15] CMS Collaboration, "Combined results of searches for the standard model Higgs boson in pp collisions at sqrt(s) = 7 TeV", *Phys. Lett. B* **710** (2012) 26–48, doi:10.1016/j.physletb.2012.02.064, arXiv:1202.1488.

[16] ATLAS Collaboration, "Combined search for the Standard Model Higgs boson using up to 4.9 fb^{-1} of pp collision data at $\sqrt{s} = 7$ TeV with the ATLAS detector at the LHC", *Phys. Lett. B* **710** (2012) 49–66, doi:10.1016/j.physletb.2012.02.044, arXiv:1202.1408.

[17] ATLAS Collaboration, "Combined search for the Standard Model Higgs boson in pp collisions at sqrt(s) = 7 TeV with the ATLAS detector", *Phys. Rev. D* **86** (2012) 032003, doi:10.1103/PhysRevD.86.032003, arXiv:1207.0319.

[18] ALEPH, DELPHI, L3, OPAL Collaborations, and the LEP Working Group for Higgs boson searches, "Search for the standard model Higgs boson at LEP", *Phys. Lett. B* **565** (2003) 61, doi:10.1016/S0370-2693(03)00614-2, arXiv:hep-ex/0306033.

[19] CMS Collaboration, "Observation of Z decays to four leptons with the CMS detector at LHC", arXiv:1210.3844. Submitted to Journal of High Energy Physics.

[20] CMS Collaboration, "The CMS experiment at the CERN LHC", *JINST* **3** (2008) S08004, doi:10.1088/1748-0221/3/08/S08004.

[21] CMS Collaboration, "Particle-Flow Event Reconstruction in CMS and Performance for Jets, Taus, and MET", CMS Physics Analysis Summary CMS-PAS-PFT-09-001, (2009).

[22] CMS Collaboration, "Commissioning of the Particle–Flow reconstruction in Minimum–Bias and Jet Events from pp Collisions at 7 TeV", CMS Physics Analysis Summary CMS-PAS-PFT-10-002, (2010).

[23] S. Baffioni et al., "Electron reconstruction in CMS", *Eur. Phys. J. C* **49** (2007) 1099, doi:10.1140/epjc/s10052-006-0175-5.

[24] CMS Collaboration, "Electron reconstruction and identification at $\sqrt{s} = 7$ TeV", CMS Physics Analysis Summary CMS-PAS-EGM-10-004, (2010).

[25] CMS Collaboration, "Performance of CMS muon reconstruction in pp collision events at sqrt(s) = 7 TeV", *JINST* **7** (2012) P10002, doi:10.1088/1748-0221/7/10/P10002, arXiv:1206.4071.

[26] CMS Collaboration, "Commissioning of the particle-flow event reconstruction with leptons from J/ψ and W decays at 7 TeV", CMS Physics Analysis Summary CMS-PAS-PFT-10-003, (2010).

[27] CMS Collaboration, "Performance of tau-lepton reconstruction and identification in CMS", *JINST* **7** (2012) P01001, doi:10.1088/1748-0221/7/01/P01001, arXiv:1109.6034.

[28] M. Cacciari and G. P. Salam, "Pileup subtraction using jet areas", *Phys. Lett. B* **659** (2008) 119, doi:10.1016/j.physletb.2007.09.077, arXiv:0707.1378.

[29] CMS Collaboration, "Measurement of the Inclusive W and Z Production Cross Sections in pp Collisions at $\sqrt{s} = 7$ TeV", *JHEP* **10** (2011) 132, doi:10.1007/JHEP10(2011)132.

[30] S. Frixione, P. Nason, and C. Oleari, "Matching NLO QCD computations with Parton Shower simulations: the POWHEG method", *JHEP* **11** (2007) 070, doi:10.1088/1126-6708/2007/11/070, arXiv:0709.2092.

[31] Y. Gao et al., "Spin determination of single-produced resonances at hadron colliders", *Phys. Rev. D* **81** (2010) 075022, doi:10.1103/PhysRevD.81.075022, arXiv:1001.3396.

[32] G. Passarino, C. Sturm, and S. Uccirati, "Higgs Pseudo-Observables, Second Riemann Sheet and All That", *Nucl. Phys. B* **834** (2010) 77, doi:10.1016/j.nuclphysb.2010.03.013, arXiv:1001.3360.

[33] S. Goria, G. Passarino, and D. Rosco, "The Higgs Boson Lineshape", *Nucl. Phys. B* **864** (2012) 530–579, doi:10.1016/j.nuclphysb.2012.07.006, arXiv:1112.5517.

[34] N. Kauer and G. Passarino, "Inadequacy of zero-width approximation for a light Higgs boson signal", *JHEP* **1208** (2012) 116, doi:10.1007/JHEP08(2012)116, arXiv:1206.4803.

[35] G. Passarino, "Higgs Interference Effects in gg $\to$ ZZ and their Uncertainty", *JHEP* **1208** (2012) 146, doi:10.1007/JHEP08(2012)146, arXiv:1206.3824.

[36] N. Kauer, "Signal-background interference in gg -gt; H -gt; VV", arXiv:1201.1667.

[37] T. Sjöstrand, S. Mrenna, and P. Z. Skands, "PYTHIA 6.4 Physics and Manual", *JHEP* **05** (2006) 026, doi:10.1088/1126-6708/2006/05/026, arXiv:hep-ph/0603175.

[38] C. Anastasiou, R. Boughezal, and F. Petriello, "Mixed QCD-electroweak corrections to Higgs boson production in gluon fusion", *JHEP* **04** (2009) 003, doi:10.1088/1126-6708/2009/04/003, arXiv:0811.3458.

[39] D. de Florian and M. Grazzini, "Higgs production through gluon fusion: updated cross sections at the Tevatron and the LHC", *Phys. Lett. B* **674** (2009) 291, doi:10.1016/j.physletb.2009.03.033, arXiv:0901.2427.

[40] J. Baglio and A. Djouadi, "Higgs production at the LHC", *JHEP* **03** (2011) 055, doi:10.1007/JHEP03(2011)055, arXiv:1012.0530.

[41] LHC Higgs Cross Section Working Group, "Handbook of LHC Higgs Cross Sections: 1. Inclusive Observables", CERN Report CERN-2011-002, (2011).

[42] A. Djouadi, M. Spira, and P. M. Zerwas, "Production of Higgs bosons in proton colliders: QCD corrections", *Phys. Lett. B* **264** (1991) 440–446, doi:10.1016/0370-2693(91)90375-Z.

[43] S. Dawson, "Radiative corrections to Higgs boson production", *Nucl. Phys. B* **359** (1991) 283, doi:10.1016/0550-3213(91)90061-2.

[44] M. Spira et al., "Higgs boson production at the LHC", *Nucl. Phys. B* **453** (1995) 17, doi:10.1016/0550-3213(95)00379-7, arXiv:hep-ph/9504378.

[45] R. V. Harlander and W. B. Kilgore, "Next-to-next-to-leading order Higgs production at hadron colliders", *Phys. Rev. Lett.* **88** (2002) 201801, doi:10.1103/PhysRevLett.88.201801, arXiv:hep-ph/0201206.

[46] C. Anastasiou and K. Melnikov, "Higgs boson production at hadron colliders in NNLO QCD", *Nucl. Phys. B* **646** (2002) 220, doi:10.1016/S0550-3213(02)00837-4, arXiv:hep-ph/0207004.

[47] V. Ravindran, J. Smith, and W. L. van Neerven, "NNLO corrections to the total cross section for Higgs boson production in hadron-hadron collisions", *Nucl. Phys. B* **665** (2003) 325, doi:10.1016/S0550-3213(03)00457-7, arXiv:hep-ph/0302135.

[48] S. Catani et al., "Soft-gluon resummation for Higgs boson production at hadron colliders", *JHEP* **07** (2003) 028, doi:10.1088/1126-6708/2003/07/028, arXiv:hep-ph/0306211.

[49] S. Actis et al., "NLO Electroweak Corrections to Higgs Boson Production at Hadron Colliders", *Phys. Lett. B* **670** (2008) 12, doi:10.1016/j.physletb.2008.10.018, arXiv:0809.1301.

[50] M. Ciccolini, A. Denner, and S. Dittmaier, "Strong and electroweak corrections to the production of Higgs + 2-jets via weak interactions at the LHC", *Phys. Rev. Lett.* **99** (2007) 161803, doi:10.1103/PhysRevLett.99.161803, arXiv:0707.0381.

[51] M. Ciccolini, A. Denner, and S. Dittmaier, "Electroweak and QCD corrections to Higgs production via vector-boson fusion at the LHC", *Phys. Rev. D* **77** (2008) 013002, doi:10.1103/PhysRevD.77.013002, arXiv:0710.4749.

[52] T. Figy, C. Oleari, and D. Zeppenfeld, "Next-to-leading order jet distributions for Higgs boson production via weak-boson fusion", *Phys. Rev. D* **68** (2003) 073005, doi:10.1103/PhysRevD.68.073005, arXiv:hep-ph/0306109.

[53] K. Arnold et al., "VBFNLO: A parton level Monte Carlo for processes with electroweak bosons", *Comput. Phys. Commun.* **180** (2009) 1661, doi:10.1016/j.cpc.2009.03.006, arXiv:0811.4559.

[54] P. Bolzoni et al., "Higgs production via vector-boson fusion at NNLO in QCD", *Phys. Rev. Lett.* **105** (2010) 011801, doi:10.1103/PhysRevLett.105.011801, arXiv:1003.4451.

[55] A. Bredenstein et al., "Precise predictions for the Higgs-boson decay H $\to$ WW/ZZ $\to$ 4 leptons", *Phys. Rev. D* **74** (2006) 013004, doi:10.1103/PhysRevD.74.013004, arXiv:hep-ph/0604011.

[56] A. Bredenstein et al., "Radiative corrections to the semileptonic and hadronic Higgs-boson decays H $\to$W W / Z Z$\to$ 4 fermions", *JHEP* **02** (2007) 080, doi:10.1088/1126-6708/2007/02/080, arXiv:hep-ph/0611234.

[57] A. Djouadi, J. Kalinowski, and M. Spira, "HDECAY: A program for Higgs boson decays in the standard model and its supersymmetric extension", *Comput. Phys. Commun.* **108** (1998) 56, doi:10.1016/S0010-4655(97)00123-9, arXiv:hep-ph/9704448.

[58] S. Actis et al., "NNLO Computational Techniques: the Cases $H \to \gamma\gamma$ and $H \to gg$", *Nucl. Phys. B* **811** (2009) 182, doi:10.1016/j.nuclphysb.2008.11.024, arXiv:0809.3667.

[59] J. Alwall et al., "MadGraph/MadEvent v4: The New Web Generation", *JHEP* **09** (2007) 028, doi:10.1088/1126-6708/2007/09/028, arXiv:0706.2334.

[60] T. Binoth, N. Kauer, and P. Mertsch, "Gluon-induced QCD corrections to $pp \to ZZ \to \ell\bar{\ell}\ell'\bar{\ell}'$", in *Proceedings of the XVI Int. Workshop on Deep-Inelastic Scattering and Related Topics (DIS'07)*. 2008. arXiv:0807.0024. doi:10.3360/dis.2008.142.

[61] H.-L. Lai et al., "Uncertainty induced by QCD coupling in the CTEQ global analysis of parton distributions", *Phys. Rev. D* **82** (2010) 054021, doi:10.1103/PhysRevD.82.054021, arXiv:1004.4624.

[62] H.-L. Lai et al., "New parton distributions for collider physics", *Phys. Rev. D* **82** (2010) 074024, doi:10.1103/PhysRevD.82.074024, arXiv:1007.2241.

[63] J. Allison et al., "Geant4 developments and applications", *IEEE Trans. Nucl. Sci.* **53** (2006) 270, doi:10.1109/TNS.2006.869826.

[64] A. Soni and R. Xu, "Probing CP violation via Higgs decays to four leptons", *Phys. Rev. D* **48** (1993) 5259–5263, doi:10.1103/PhysRevD.48.5259, arXiv:hep-ph/9301225.

[65] V. D. Barger, K.-m. Cheung, A. Djouadi et al., "Higgs bosons: Intermediate mass range at e+ e- colliders", *Phys. Rev. D* **49** (1994) 79–90, doi:10.1103/PhysRevD.49.79, arXiv:hep-ph/9306270.

[66] S. Y. Choi, D. J. Miller, M. M. Muhlleitner et al., "Identifying the Higgs spin and parity in decays to Z pairs", *Phys. Lett. B* **553** (2003) 61–71, doi:10.1016/S0370-2693(02)03191-X, arXiv:hep-ph/0210077.

[67] B. Allanach, K. Odagiri, M. Palmer et al., "Exploring small extra dimensions at the large hadron collider", *JHEP* **0212** (2002) 039, arXiv:hep-ph/0211205.

[68] C. P. Buszello, I. Fleck, P. Marquard et al., "Prospective analysis of spin- and CP-sensitive variables in $H \to ZZ \to l(1)^+l(1)^-l(2)^+l(2)^-$ at the LHC", *Eur.Phys.J.* **C32** (2004) 209–219, doi:10.1140/epjc/s2003-01392-0, arXiv:hep-ph/0212396.

[69] R. M. Godbole, D. J. Miller, and M. M. Muhlleitner, "Aspects of CP violation in the H ZZ coupling at the LHC", *JHEP* **0712** (2007) 031, doi:10.1088/1126-6708/2007/12/031, arXiv:0708.0458.

[70] W.-Y. Keung, I. Low, and J. Shu, "Landau-Yang Theorem and Decays of a Z' Boson into Two Z Bosons", *Phys. Rev. Lett.* **101** (2008) 091802, doi:10.1103/PhysRevLett.101.091802, arXiv:0806.2864.

[71] O. Antipin and A. Soni, "Towards establishing the spin of warped gravitons", *JHEP* **0810** (2008) 018, doi:10.1088/1126-6708/2008/10/018, arXiv:0806.3427.

[72] K. Hagiwara, Q. Li, and K. Mawatari, "Jet angular correlation in vector-boson fusion processes at hadron colliders", *JHEP* **0907** (2009) 101, doi:10.1088/1126-6708/2009/07/101, arXiv:0905.4314.

[73] A. De Rujula, J. Lykken, M. Pierini et al., "Higgs look-alikes at the LHC", *Phys. Rev. D* **82** (2010) 013003, doi:10.1103/PhysRevD.82.013003, arXiv:1001.5300.

[74] J. S. Gainer, K. Kumar, I. Low et al., "Improving the sensitivity of Higgs boson searches in the golden channel", *JHEP* **1111** (2011) 027, doi:10.1007/JHEP11(2011)027, arXiv:1108.2274.

[75] S. Bolognesi, Y. Gao, A. V. Gritsan et al., "On the spin and parity of a single-produced resonance at the LHC", arXiv:1208.4018.

[76] Y. Chen, N. Tran, and R. Vega-Morales, "Scrutinizing the Higgs Signal and Background in the $2e2\mu$ Golden Channel", arXiv:1211.1959.

[77] J. M. Campbell and R. K. Ellis, "MCFM for the Tevatron and the LHC", *Nucl. Phys. Proc. Suppl.* **205** (2010) 10, doi:10.1016/j.nuclphysbps.2010.08.011, arXiv:1007.3492.

[78] J. M. Campbell and R. K. Ellis, "An update on vector boson pair production at hadron colliders", *Phys. Rev. D* **60** (1999) 113006, doi:10.1103/PhysRevD.60.113006, arXiv:hep-ph/9905386.

[79] J. M. Campbell, R. Ellis, and C. Williams, "Vector boson pair production at the LHC", *JHEP* **07** (2011) 018, doi:10.1007/JHEP07(2011)018, arXiv:1105.0020.

[80] A. Belyaev, N. D. Christensen, and A. Pukhov, "CalcHEP 3.4 for collider physics within and beyond the Standard Model", arXiv:1207.6082.

[81] P. Avery, D. Bourilkov, M. Chen et al., "Precision Studies of the Higgs Golden Channel H $\rightarrow$ ZZ* $\rightarrow$ 4l. Part I. Kinematic discriminants from leading order matrix elements", arXiv:1210.0896.

[82] M. Botje et al., "The PDF4LHC Working Group Interim Recommendations", (2011). arXiv:1101.0538.

[83] S. Alekhin et al., "The PDF4LHC Working Group Interim Report", (2011). arXiv:1101.0536.

[84] H.-L. Lai et al., "New parton distributions for collider physics", *Phys. Rev. D* **82** (2010) 074024, doi:10.1103/PhysRevD.82.074024, arXiv:1007.2241.

[85] A. Martin et al., "Parton distributions for the LHC", *Eur. Phys. J. C* **63** (2009) 189, doi:10.1140/epjc/s10052-009-1072-5, arXiv:0901.0002.

[86] R. D. Ball et al., "Impact of Heavy Quark Masses on Parton Distributions and LHC Phenomenology", *Nucl. Phys. B* **849** (2011) 296, doi:10.1016/j.nuclphysb.2011.03.021, arXiv:1101.1300.

[87] CMS Collaboration, "Absolute Calibration of the CMS Luminosity Measurement: Summer 2011 Update", CMS Physics Analysis Summary CMS-PAS-EWK-11-001, (2011).

[88] ATLAS and CMS Collaborations, LHC Higgs Combination Group, "Procedure for the LHC Higgs boson search combination in Summer 2011", ATL-PHYS-PUB/CMS NOTE 2011-11, 2011/005, (2011).

[89] T. Junk, "Confidence level computation for combining searches with small statistics", *Nucl. Instrum. Meth. A* **434** (1999) 435, doi:10.1016/S0168-9002(99)00498-2, arXiv:hep-ex/9902006.

[90] A. Read, "Modified frequentist analysis of search results (the CL_s method)", Technical Report CERN-OPEN-2000-005, CERN, (2000).

[91] Particle Data Group, "Review of particle physics", *J. Phys. G* **37** (2010) 075021, doi:10.1088/0954-3899/37/7A/075021.

[92] M. Oreglia, "A study of the reactions $\psi' \rightarrow \gamma\gamma\psi$". PhD thesis, Stanford University, 1980. SLAC-0236.